Title

[11C]acetate PET Imaging is not Always Associated with Increased Lipogenesis in Hepatocellular Carcinoma in Mice

Journal

Molecular Imaging and Biology, 18(3)

ISSN

1536-1632

Authors

Li, Lei
Che, Li
Wang, Chunmei
et al.

Publication Date

2016-06-01

DOI

10.1007/s11307-015-0915-8

Peer reviewed

HHS Public Access

Author manuscript

Mol Imaging Biol. Author manuscript; available in PMC 2016 June 01.

Published in final edited form as:

Mol Imaging Biol. 2016 June ; 18(3): 360–367. doi:10.1007/s11307-015-0915-8.

[^{11}C]acetate PET Imaging is not Always Associated with Increased Lipogenesis in Hepatocellular Carcinoma in Mice

Lei Li[1,2], **Li Che**[2], **Chunmei Wang**[2], **Joseph E. Blecha**[3], **Xiaolei Li**[2], **Henry F. VanBrocklin**[3], **Diego F. Calvisi**[4], **Michelle Puchowicz**[5], **Xin Chen**[2], and **Youngho Seo**[3,6,7,8]

[1]School of Pharmacy, Tongji Medical College, Huazhong University of Science and Technology, Wuhan, Hubei, China

[2]Department of Bioengineering and Therapeutic Sciences, University of California, San Francisco, CA, U.S.A.

[3]Department of Radiology and Biomedical Imaging, University of California, San Francisco, CA, U.S.A.

[4]Institute of Pathology, University of Greifswald, Greifswald, Germany

[5]Department of Nutrition, Case Western Reserve University, Cleveland, OH, U.S.A.

[6]Department of Radiation Oncology, University of California, San Francisco, CA, U.S.A.

[7]UCSF-UC Berkeley Joint Graduate Group in Bioengineering, University of California, San Francisco, CA, U.S.A.

[8]Molecular Biophysics and Integrated Bioimaging Division, Lawrence Berkeley National Laboratory, Berkeley, CA, U.S.A.

Abstract

Purpose—Altered metabolism, including increased glycolysis and *de novo* lipogenesis, is one of the hallmarks of cancer. Radiolabeled nutrients, including glucose and acetate, are extensively used for the detection of various tumors, including hepatocellular carcinomas (HCCs). High signal of [^{11}C]acetate positron emission tomography (PET) in tumors is often considered to be associated with increased expression of Fatty Acid Synthase (FASN) and increased *de novo* lipogenesis in tumor tissues. Defining a subset of tumors with increased [^{11}C]acetate PET signal and thus increased lipogenesis was suggested to help select a group of patients, who may benefit from lipogenesis-targeting therapies.

Procedures—To investigate whether [^{11}C]acetate PET imaging is truly associated with increased *de novo* lipogenesis along with hepatocarcinogenesis, we performed [^{11}C]acetate PET imaging in wildtype mice as well as two mouse HCC models, induced by myrAKT/Ras^{V12} (AKT/

Corresponding author: Youngho Seo, UCSF Physics Research Laboratory, Department of Radiology and Biomedical Imaging, University of California, San Francisco, California 94143-0946. youngho.seo@ucsf.edu; telephone:+1(415)-3539464; Fax: +1(415)-3539423 or Xin Chen, Dept. of Bioengineering and Therapeutic Sciences; University of California, San Francisco, California 94143-0912. xin.chen@ucsf.edu; telephone: +1(415)-5026526; Fax:+1(415)-5024322.

Conflict of Interest

The authors declare that they have no conflict of interest.

Ras) and PIK3CA^{1047R}/c-Met (PI3K/Met) oncogene combinations. In addition, we analyzed FASN expression and *de novo* lipogenesis rate in these mouse liver tissues.

Results—We found that while HCCs induced by AKT/Ras co-expression showed high levels of [^{11}C]acetate PET signal compared to normal liver, HCCs induced by PI3K/Met overexpression did not. Intriguingly, elevated FASN expression and increased *de novo* lipogenesis rate were observed in both AKT/Ras and PI3K/Met HCCs.

Conclusion—Altogether, our study suggests that [^{11}C]acetate PET imaging can be a useful tool for imaging of a subset of HCCs. However, at molecular level, the increased [^{11}C]acetate PET imaging is not always associated with increased FASN expression or *de novo* lipogenesis.

Keywords

[^{11}C]acetate; PET; fatty acid synthase expression; *de novo* lipogenesis; hepatocellular carcinoma

Introduction

Hepatocellular carcinoma (HCC) is a solid tumor associated with high mortality rate, due to the limited treatment options available against this disease. According to the statistics provided by American Cancer Society, the 5-year survival rate between 2001 and 2007 for all liver cancers is only 14% [1]. The prognosis is even more unfavorable (4% 5-year survival rate) when the cancer spreads to distant sites [2].

Alteration of metabolism, including elevated glycolysis and *de novo* lipogenesis is one of hallmarks of cancer. Fatty acid synthase (FASN) catalyzes the final step in the conversion of carbohydrates to palmitate, and is therefore essential for mammalian lipogenesis. Although one might expect tumors to be able to take up dietary fat, virtually all solid tumors of epithelial origin require FASN for survival and proliferation [3-9]. Increased expression of FASN is a hallmark of all major epithelial cancers (for review see [10]) and is usually associated with poor prognosis [4-5, 11-14]. A blockade of FASN by siRNA-mediated knockdown or covalent inhibitors arrests the tumor cell cycle at G1/S and causes tumor cell apoptosis [9, 15-19]. Another study suggests that up-regulation of FASN may even be oncogenic [20]. Recent studies show a strong link between lipogenesis, FASN, and HCC [21-27]. A previous report from our group demonstrated that *de novo* lipogenesis and FASN levels increase as hepatocytes progress from non-tumorigenic to HCC [22]. This change in lipogenic phenotype correlates with activation of AKT/mTOR/RSP6 signaling cascades in human HCC[22].

The aberrant metabolic program of tumor cells has led to the development of metabolic imaging systems. For instance, the finding of increased glucose utilization by cancer cells has been successfully used to develop the 2-deoxy-2-[^{18}F]fluoro-D-deoxyglucose PET ([^{18}F]FDG PET), one of the most widely used cancer imaging modalities. However, imaging of HCC by [^{18}F]FDG PET has resulted in mixed results. It was reported that 30-50% of HCC are negative for [^{18}F]FDG PET [28-30]. The variable expression of glucose-6-phosphatase, the enzyme responsible for the conversion of glucose-6-phosphate back into glucose, and increased reliance of HCCs on other metabolic substrates than glucose, can be

among the factors responsible for the variability of [^{18}F]FDG PET imaging results. Another imaging metabolic agent, [^{11}C]acetate, has been proven to be useful for the imaging of various malignancies, including HCCs [31-32]. When the dual-tracer [^{18}F]FDG / [^{11}C]acetate PET imaging is adopted for imaging HCC in places where [^{11}C]acetate PET can be performed, sensitivity and specificity have greatly improved [28, 33-35]. Interestingly, most of HCC tumors with weak glucose utilization (unmarked [^{18}F]FDG uptake) have elevated [^{11}C]acetate uptake [32, 36].

Although clinically [^{11}C]acetate is widely used for the evaluation of myocardial oxidative metabolism [37-38], the observed relationship between radioactive acetate uptake and lipid biosynthesis suggested that increased acetate uptake in malignancies can be associated with fatty acid biosynthesis and serve as a measure of the intensity of lipid biosynthesis in tumors [36]. Indeed, incorporation of [^{14}C]acetate in lipid-soluble fraction correlates with the rate of cell proliferation in various cancer cell lines [39]. In particular, the uptake of [^{11}C]acetate correlates with the expression of FASN in prostate cancer cells both *in vitro* and in xenografts, and is blocked by a FASN inhibitor [36]. In addition, the inhibition of the expression of cytosolic acetyl-CoA synthetase (ACSS2), the enzyme responsible for the incorporation of acetate into lipids [40], decreases the incorporation of [^{14}C]acetate into various cancer cell lines [41]. However, together with the initial use of radiolabeled acetate to evaluate the oxidative metabolism, [^{14}C]acetate is shown to be catabolized into CO_2 and is incorporated into amino acids in various cancer cell lines [39], suggesting its role as a precursor for the Krebs cycle activity. The latter role of acetate in tumors is also supported by the association of the increased [^{11}C]acetate uptake with the increased expression of mitochondrial acetyl-CoA synthetase (ACSS1) [42]. Altogether, the studies published so far suggest that increased uptake and catabolism of radiolabeled acetate in tumors is not necessarily associated with its increased utilization for lipid biosynthesis.

In order to objectively study the correlation between *de novo* lipogenesis and [^{11}C]acetate uptake *in vivo* in HCC, we have employed two murine liver tumor models in which tumors were induced by the ectopic expression of oncogenes often observed in human HCCs, either by a combination of myrAKT and Ras^{V12} (hereinafter, AKT/Ras) or by PIK3CA^{1047R} and c-Met (hereinafter, PI3K/Met). In these models, we performed *in vivo* PET imaging of [^{11}C]acetate followed by quantification of [^{11}C]acetate PET uptake by dynamic imaging and kinetic modeling, as well as evaluated the extent of lipogenesis.

Materials And Methods

Constructs and reagents

The constructs used for mouse injection, including pT3-EF1α-myrAKT, pT2-Caggs-NRasV12, pT3-EF1α-c-Met, and pCMV/sleeping beauty transposase (pCMV/SB), were described previously [43-44]. Human PIK3CA with H1047R mutation (Addgene plasmid 12524) was cloned into pT3-EF1α vector via the Gateway PCR cloning strategy (Invitrogen, Carlsbad, CA). All plasmids were purified using the Endotoxin free Maxi prep kit (Sigma, St.Louis, MO) before being injected into the mice. ^2H_2O was purchased from Sigma. The [^{11}C]acatete was synthesized by trapping the $^{11}CO_2$ in a methyl magnesium bromide solution and then distillation into saline [45] at the radiochemistry/radiopharmacy facility at

the University of California, San Francisco (UCSF). Radiosynthesis and quality control processes followed standard procedures established at the facility.

Hydrodynamic injection and mouse monitoring

Wild-type FVB/N mice were obtained from Charles River (Wilmington, MA). Hydrodynamic injection was performed as described [46]. In brief, 10μg pT3-EF1α-myrAKT and 10μg pT2-Caggs-NRasV12 were mixed with pCMV/SB in a ratio of 25:1. Similarly, 10μg pT3-EF1α-c-Met and 10μg pT3-EF1α-PIK3CAH104R were mixed with pCMV/SB. The plasmid mixture was diluted in 2 ml saline (0.9% NaCl), filtered through 0.22 μm filter, and injected into the lateral tail vein of 6 to 8-week-old FVB/N mice in 5 to 7 seconds. Mice were monitored two times per week for liver tumor development as palpable abdominal mass. All mouse procedures, including housing, feeding and monitoring were performed based on the protocol approved by UCSF Institutional Animal Care and Use Committee.

Immunohistochemical staining

Upon euthanasia, mouse liver tissues were collected and fixed in 4% paraformaldehyde (PFA) overnight at 4°C and embedded in paraffin. For antigen retrieval, slides were put into 10 mM sodium citrate buffer (pH 6.0), and placed in a microwave on high for 10 min. Slides were blocked with 5% goat serum and the Avidin-Biotin blocking kit (Vector Laboratories, Burlingame, CA). Primary antibodies were added to the slides and incubated overnight at 4°C. Slides were washed and incubated with a biotin conjugated secondary antibody. Detection was performed with the ABC-Elite peroxidase kit (Vector Laboratories) using the DAB as the substrate. Primary antibodies used in the study include: Anti-FASN and anti-acetyl-CoA carboxylase (anti-ACC) antibodies; both were obtained from Cell Signaling Technology Inc.

Oil-Red-O staining

The Oil Red O stain kit (American MasterTech) was used for the Oil Red O staining, following the instruction provided by the manufacturer.

Lipid analysis

Lipid analysis was performed by the Vanderbilt University MMPC/DRTC Lipid Core as described in our previous publication [47].

Measurement of *de novo* lipogenesis rate in mouse liver tumor samples

Wild type FVB/N mice or tumor bearing mice (with palpable abdominal mass) were injected with a single bolus dose of $^{2}H_2O$ to achieve target total body water enrichment of 4.0% ^{2}H-water. The amount of $^{2}H_2O$ was estimated based on total body weight of which about 70% is approximately body water. This value was then multiplied by 4% to yield the amount of heavy water to be injected as a single bolus (thus, a 30 g mouse would receive 0.84 ml of heavy water). Mice were euthanized 8 hours after D_20 injection. Blood was collected and liver tissues were snap frozen in liquid nitrogen.

In vivo *de novo* lipogenesis was measured using the deuterium oxide (^2H_2O) water method [48-50-] by the Case Western Reserve University Mouse Phenotyping Center. Total triglyceride-bound palmitate was isolated from tissues by chemical hydrolysis and extraction procedures and analyzed by gas chromatography mass spectrometry (GC-MS). The percent label of ^{2}H-labeled palmitate largely reflects the pool of newly synthesized lipids.[50] Thus, as a result of the measured percent of ^{2}H-label incorporation into palmitate, *de novo* lipogenesis is then calculated. For the calculation, the contribution of *de novo* lipogenesis to the pool of triglyceride and palmitate was calculated using the following equation: % newly made palmitate = [total ^{2}H-labeled palmitate • (^{2}H-labeled body water × n)$^{-1}$] × 100, where n is the number of exchangeable hydrogens, which is assumed to 22 [48-49]. ^{2}H Labeling *of Body Water*—^{2}H-labeled total body water enrichment was measured from the blood collected from each mouse and determined using the acetone exchange where the ^{2}H-label in acetone, as measured by GC-MS, reflects the enrichment of total body water [50.

Animal imaging protocol

All *in vivo* animal imaging was performed using a microPET/CT scanner (Inveon dedicated PET (DPET) docked with CT in the multimodality (MM) platform, Siemens Medical Solutions USA, Inc., Malvern, PA). Murine PET/CT imaging followed established standard operating procedures approved by the UCSF Institutional Animal Care and Use Committee (IACUC) and Laboratory Animal Resource Center (LARC).

Tumor imaging using [^{11}C]acetate was performed when the liver tumors were palpable, meaning substantial growth was apparent. After the *in vivo* imaging sessions and the radionuclides decayed to background, the animals were euthanized and the presence of liver tumors was confirmed by visual investigation. For all animal procedures, a custom-made mouse tail vein catheter consisting of a 28-gauge needle and a 100-150 mm long polyethylene microtubing (PE/1, Scientific Commodities, Inc., Lake Havasu City, AZ) was placed through the tail vein to ensure intravenous administration of radiotracers. The absence of leakage and misinjection was verified for all microPET/CT scans by whole-body inspection of reconstructed PET images. Animals were maintained under 1-2% isoflurane anesthesia during radiotracer administration and imaging sessions. All animals were also fasted overnight before the day of each imaging session. For the [^{11}C]acetate imaging, 6.81 – 15.54 MBq was administered to five AKT/Ras and three PI3K/Met mice intravenously, immediately followed by thirty minutes of dynamic multiframe PET data acquisitions. The catheter was placed before the animals were transported to the microPET/CT scanner, and before the [^{11}C]-acetate administration, the catheter placement within the vein was confirmed by flushing a small amount of saline. The same dynamic PET imaging protocol was applied to additional six FVB/N normal mice for control measurements of the influx rate constant measurements of acetate metabolism.

[^{11}C]acetate PET data were reconstructed using a three-dimensional ordered-subsets expectation maximization (3D OS-EM) with maximum a posteriori (MAP) algorithm provided by the manufacturer. CT-based attenuation correction was incorporated in PET reconstruction algorithms. Dynamic PET data were reconstructed into dynamic multiframes (5s×6, 10s×6, 30s×3, 60s×7, 600s×2) using the same reconstruction algorithm. The scan

parameters for *in vivo* microCT were 120 projections of continuous rotations to cover 220° with an x-ray tube operated at 80 kVp, 0.5 mA, and 175 ms exposure time. The CT data were reconstructed using a modified cone-beam Feldkamp reconstruction algorithm (COBRA, Exxim Computing Corporation, Pleasanton, CA). For visualization of the 3D distribution of [^{11}C]acetate metabolism, volume rendering of registered [^{11}C]acetate PET over CT was performed using Amira (FEI, Hillsboro, OR).

PET image analysis

A two-tissue irreversible compartment model was used to derive influx rate constants (K_i) from dynamic PET data of [^{11}C]acetate. Instead of nonlinear curve-fitting of one blood compartment and two tissue compartments, a linear-fitting graphical method of Patlak analysis [51] was employed to derive voxel-by-voxel K_i values, and the mean value of K_i values in voxels enclosed by tumor ROIs. One drawback of adopting the two-tissue irreversible compartment model for [^{11}C]acetate would be that if [^{11}C]acetate is metabolized to [^{11}C]CO_2 through the Krebs cycle, it can draw complications in deriving the influx rate constant using the Patlak graphical method for which metabolized [^{11}C]acetate is assumed to be trapped in the tumor [52]. However, since our goal of using [^{11}C]acetate PET imaging for this study is to quantify how much catabolism of [^{11}C]acetate in tumors and normal liver tissues, the approach of using a generic irreversible two compartment model still provides the values (K_i's) that are related to [^{11}C]acetate metabolism as a whole.

We used a commercially available software package (Inveon Research Workplace 2.0, Siemens Medical Solutions USA, Inc., Malvern, PA) for all analyses included in this manuscript. For the kinetic modeling of [^{11}C]acetate data, the blood input function was also derived from the left ventricular myocardial blood pool in reconstructed PET images. We used a small volume of interest, typically encompassing 2-3 voxels, well within the left ventricular chamber for the input function derivation in order to minimize partial volume effect from the myocardial uptake of [^{11}C]acetate as well as the spill-over effect of the blood pool uptake. No other partial volume error compensation technique was used.

Statistical Analysis

All data were analyzed with Prism 6 (GraphPad, San Diego, CA). Comparisons were performed with two-tailed unpaired *t* test or Newman-Keuls multiple comparison test.

Results

Increased *de novo* lipogenesis in AKT/Ras and PI3K/Met induced liver tumors

In our recent studies, we demonstrated that in humans, *de novo* lipogenesis and FASN increase as hepatocytes progress from non-tumorigenic to full malignancy [22]. This change in lipogenic phenotype correlates with activation of AKT/mTOR/RSP6 signaling cascade [22]. Furthermore, our studies suggested coordinated activation of AKT/mTOR and Ras/MAPK pathways in the subset of human HCCs with aggressive phenotypes [53]. To study the biochemical crosstalk between the two pathways, we developed a murine liver tumor models with activated AKT/mTOR and Ras/MAPK pathways via hydrodynamically co-transfecting myr-AKT and NRasV12 proto-oncogenes (hereinafter, AKT/Ras) [43].

AKT/Ras injected mice developed lethal burden of liver tumors by 5 to 6 weeks post-injection. Histologically, tumors are comprised of poorly differentiated HCC with small percentage of cholangiocarcinoma (CCA) or mixed HCC/CCA (Fig. 1a). Tumor cells showed concomitant activation of AKT/mTOR and Ras/MAPK cascades [43].

Activating mutations of PIK3CA are found in approximately 4% of human HCC samples (COSMIC database); among them PIK3CAH1047R is one of the most common PIK3CA mutations. Overexpression and activation of c-Met is one of the most frequently observed biochemical events in HCC [54]. Thus, we developed another murine HCC model by hydrodynamically co-transfecting PIK3CAH1047R and c-Met (hereinafter PI3K/Met). PI3K/Met co-expression induced HCC formation by ~15 weeks post injection (Fig. 1a). The detailed description of this murine HCC model will be presented in a separated manuscript (Wang C, manuscript in preparation). Importantly, PI3K/Met liver tumors showed elevated AKT and Ras pathway activation (data not shown). Therefore, these mice provide another useful murine HCC model to study the molecular events associated with activation of AKT/mTOR and Ras/MAPK cascades in hepatocarcinogenesis.

As both AKT/Ras and PI3K/Met liver tumors have high levels of AKT/mTOR pathway, we investigated whether lipogenic pathway is activated in these murine liver tumor models. Indeed, we found large lipid droplet accumulation in tumor cells in both mouse models (Fig. 1b). Consistently, AKT/Ras and PI3K/Met tumor cells showed high levels of total triglycerides (TG) and cholesterol esters (CE) compared to normal liver tissues (Fig. 2). To confirm that the accumulation of lipid droplets in tumors is the result of increased rate of lipogenesis, we used heavy water (^2H_2O) as the stable isotope tracer [48, 50]. The results demonstrated significantly increased *de novo* lipogenesis rate in AKT/Ras and PI3K/Met liver tumors in comparison with normal liver tissues (Fig. 3). Consistent with this, the expression of lipogenic pathway genes, including FASN and ACC, was significantly increased in AKT/Ras and PI3K/Met tumors (Fig. 1c and d).

In summary, our data demonstrate that liver tumors induced by AKT/Ras and PI3K/Met overexpression, both exhibiting the activation of the AKT/mTOR signaling, have an increased *de novo* lipogenesis rate and a profound lipid accumulation in tumor cells. Thus, these tumor models recapitulate human HCC subsets in which the increased activity of AKT/mTOR cascade correlates with increased *de novo* lipogenesis.

[^{11}C]acetate imaging in AKT/Ras and PI3K/Met liver tumor models

As increased FASN expression and *de novo* lipogenesis rate were suggested to be the molecular mechanisms underlying positive signals in [^{11}C]acetate PET/CT imaging in HCC [55-56], we imaged both tumor models with [^{11}C]acetate PET/CT. Intriguingly, we found that while AKT/Ras mice showed significant [^{11}C]acetate signal, little signal could be detected in PI3K/Met tumors in comparison with the signal from the normal liver (Fig. 4a).

The K_i values measured from dynamic [^{11}C]acetate PET/CT imaging (Fig. 4b) indicate that the acetate metabolic activity is significantly higher in AKT/Ras liver tumors (0.054 ± 0.015 min^{-1}; n = 5) in comparison with those of PI3K/Met tumors (0.0083 ± 0.0022 min^{-1}; n=3) and the normal liver (0.021 ± 0.0047 min^{-1}; n = 6). As a quality check, we also investigated

if there was any outlier measurement of K_i affected by the wide range of the administered dose of [^{11}C]acetate. We have not found any reduction of Ki values for higher dose of [^{11}C]acetate administration.

In summary, our study shows that despite the increased FASN expression and *de novo* lipogenesis rate in PI3K/Met mouse liver tumors, no significantly increased [^{11}C]acetate PET signal can be detected in these mice.

Discussion

Aberrant metabolic program has been considered a hallmark of cancer. Abnormal tumor metabolic signatures have led to the development of metabolic imaging systems, including [^{18}F]FDG and [^{11}C]acetate PET imaging. In particular, increased [^{11}C]acetate PET signal in tumors is often considered to reflect the increased *de novo* lipogenesis rate and be associated with the increased FASN expression [32-33, 55-58]. In this study, we demonstrated that out of two tumor types, induced by either AKT/Ras or PI3K/Met, while both of which had increased FASN expression and increased lipogenesis rate, only AKT/Ras tumors had significant [^{11}C]acetate PET signal. These results indicate that increased FASN expression and *de novo* lipogenesis rate are not the only factors underlying the increased [^{11}C]acetate PET/CT signal in HCCs. Indeed, as mentioned earlier, [^{11}C]acetate has been widely used to evaluate oxidative metabolism and the activity of the Krebs cycle in tissues, suggesting that increased [^{11}C]acetate PET signal in tumors can be an indicative of their increased oxidative metabolism, accompanied or not by increased lipid biogenesis. Further evaluation of acetate-derived carbon fate and its correlation with PET signal intensity is required to identify the specific mechanisms underlying the increased [^{11}C]acetate PET signal in various types of tumors. Besides the utilization in different metabolic processes, the rate of the tracer transport and clearance in different tumors versus normal tissue should be taken into account as well.

Increased imaging signal from metabolic probes including [^{11}C]acetate and [^{18}F]FDG can potentially serve not only for tumor detection but also as an indicator of the increased activity of a specific metabolic process. If the detected process is demonstrated to be required for a tumor cell proliferation and/or viability, PET imaging could then allow to stratify patients for appropriate metabolism-based therapies. However, in order to achieve this goal further thorough evaluation of mechanisms underlying increased PET signals in various tumors is required.

Having said that the complementary metabolic imaging probes are essential to further understand the specific tumor biology in malignant tumors such as HCC, the main subject of this manuscript, it is also interesting to see how [^{18}F]FDG's case in studying glucose utilization and metabolism of cancers is compared to hyperpolarized [^{13}C]pyruvate magnetic resonance spectroscopic imaging [59].

Finally, a therapeutic target based on the biochemical evidence of oncogenic pathway inhibition can be better understood and targeted if we can stratify the potential responders from nonresponders. For this purpose, the imaging probe that is linked to specific molecular

pathways will be potentially critical in the management of cancers using a molecularly-based treatment strategy [60].

Conclusion

Using mouse models of HCCs induced by AKT/Ras and PI3K/Met proto-oncogenes, we have evaluated the correlation between *de novo* lipogenesis (including the expression of the enzymes involved in *de novo* lipogenesis, FASN and ACC) and the intensity of *in vivo* [^{11}C]acetate PET signal. The data obtained from our investigation demonstrate that increased *in vivo* [^{11}C]acetate PET signal does not always correlate with increased lipid biogenesis in HCCs.

Acknowledgments

We would like to thank Mariia Yuneva for her thoughtful comments for the manuscript. We also thank Stephanie T. Murphy for her immense help on animal imaging. This work was supported in part by University of California, San Francisco (UCSF) Radiology Seed Grant, UCSF Liver Center Pilot/Feasibility Grant (P30DK026743), National Institutes of Health/National Cancer Institute (NIH/NCI) and UCSF Helen Diller Family Comprehensive Cancer Center (P30CA082103) to Youngho Seo; NIH/NCI grant (R01CA136606) to Xin Chen; NIH (U24DK76174) to Case Western Reserve University Mouse Metabolic Phenotyping Center (MMPC); National Natural Science Foundation of China (Grant No. 81201553) to Lei Li.

References

1. Siegel R, Naishadham D, Jemal A. Cancer statistics, 2012. CA Cancer J Clin. 2012; 62:10–29. [PubMed: 22237781]
2. American Cancer Society. Cancer Facts & Figures 2012. American Cancer Society; Atlanta: 2012. Selected Cancers; p. 14-15.
3. Shurbaji MS, Kalbfleisch JH, Thurmond TS. Immunohistochemical detection of a fatty acid synthase (OA-519) as a predictor of progression of prostate cancer. Human pathology. 1996; 27:917–921. [PubMed: 8816886]
4. Alo PL, Visca P, Marci A, et al. Expression of fatty acid synthase (FAS) as a predictor of recurrence in stage I breast carcinoma patients. Cancer. 1996; 77:474–482. [PubMed: 8630954]
5. Gansler TS, Hardman W 3rd, Hunt DA, et al. Increased expression of fatty acid synthase (OA-519) in ovarian neoplasms predicts shorter survival. Human Pathol. 1997; 28:686–692. [PubMed: 9191002]
6. Takahiro T, Shinichi K, Toshimitsu S. Expression of fatty acid synthase as a prognostic indicator in soft tissue sarcomas. Clin Canc Res. 2003; 9:2204–2212.
7. Visca P, Sebastiani V, Botti C, et al. Fatty acid synthase (FAS) is a marker of increased risk of recurrence in lung carcinoma. Anticanc Res. 2004; 24:4169–4173.
8. Rossi S, Ou W, Tang D, et al. Gastrointestinal stromal tumours overexpress fatty acid synthase. J Pathol. 2006; 209:369–375. [PubMed: 16583360]
9. Carvalho MA, Zecchin KG, Seguin F, et al. Fatty acid synthase inhibition with Orlistat promotes apoptosis and reduces cell growth and lymph node metastasis in a mouse melanoma model. Intl J Canc. 2008; 123:2557–2565.
10. Menendez JA, Lupu R. Fatty acid synthase and the lipogenic phenotype in cancer pathogenesis. Nat Rev Canc. 2007; 7:763–777.
11. Myers RB, Oelschlager DK, Weiss HL, et al. Fatty acid synthase: an early molecular marker of progression of prostatic adenocarcinoma to androgen independence. J Urol. 2001; 165:1027–1032. [PubMed: 11176534]
12. Bull JH, Ellison G, Patel A, et al. Identification of potential diagnostic markers of prostate cancer and prostatic intraepithelial neoplasia using cDNA microarray. Br J Canc. 2001; 84:1512–1519.

13. Rashid A, Pizer ES, Moga M, et al. Elevated expression of fatty acid synthase and fatty acid synthetic activity in colorectal neoplasia. Am J Pathol. 1997; 150:201–208. [PubMed: 9006336]
14. Alo PL, Visca P, Trombetta G, et al. Fatty acid synthase (FAS) predictive strength in poorly differentiated early breast carcinomas. Tumori. 1999; 85:35–40. [PubMed: 10228495]
15. Pizer ES, Jackisch C, Wood FD, et al. Inhibition of fatty acid synthesis induces programmed cell death in human breast cancer cells. Cancer Res. 1996; 56:2745–2747. [PubMed: 8665507]
16. Kridel SJ, Axelrod F, Rozenkrantz N, Smith JW. Orlistat is a novel inhibitor of fatty acid synthase with antitumor activity. Cancer Res. 2004; 64:2070–2075. [PubMed: 15026345]
17. Knowles LM, Axelrod F, Browne CD, Smith JW. A fatty acid synthase blockade induces tumor cell-cycle arrest by down-regulating Skp2. J Biol Chem. 2004; 279:30540–30545. [PubMed: 15138278]
18. Kridel SJ, Lowther WT, Pemble CWt. Fatty acid synthase inhibitors: new directions for oncology. Expert Opin Investig Drugs. 2007; 16:1817–1829.
19. Murata S, Yanagisawa K, Fukunaga K, et al. Fatty acid synthase inhibitor cerulenin suppresses liver metastasis of colon cancer in mice. Canc Sci. 2010; 101:1861–1865.
20. Migita T, Ruiz S, Fornari A, et al. Fatty acid synthase: a metabolic enzyme and candidate oncogene in prostate cancer. J Natl Canc Inst. 2009; 101:519–532.
21. Gao Y, Lin LP, Zhu CH, et al. Growth arrest induced by C75, A fatty acid synthase inhibitor, was partially modulated by p38 MAPK but not by p53 in human hepatocellular carcinoma. Canc Biol Ther. 2006; 5:978–985.
22. Calvisi DF, Wang C, Ho C, et al. Increased lipogenesis, induced by AKT-mTORC1-RPS6 signaling, promotes development of human hepatocellular carcinoma. Gastroenterol. 2011; 140:1071–1083.
23. Na TY, Shin YK, Roh KJ, et al. Liver X receptor mediates hepatitis B virus X protein-induced lipogenesis in hepatitis B virus-associated hepatocellular carcinoma. Hepatol. 2009; 49:1122–1131.
24. Zhu X, Qin X, Fei M, et al. Combined Phosphatase and Tensin Homolog (PTEN) Loss and Fatty Acid Synthase (FAS) Overexpression Worsens the Prognosis of Chinese Patients with Hepatocellular Carcinoma. Intl J Molec Sci. 2012; 13:9980–9991.
25. Wang Q, Zhang W, Liu Q, et al. A mutant of hepatitis B virus X protein (HBxDelta127) promotes cell growth through a positive feedback loop involving 5-lipoxygenase and fatty acid synthase. Neoplasia. 2010; 12:103–115. [PubMed: 20126469]
26. Yamashita T, Honda M, Takatori H, et al. Activation of lipogenic pathway correlates with cell proliferation and poor prognosis in hepatocellular carcinoma. J Hepatol. 2009; 50:100–110. [PubMed: 19008011]
27. Li C, Yang W, Zhang J, et al. SREBP-1 has a prognostic role and contributes to invasion and metastasis in human hepatocellular carcinoma. Intl J Molec Sci. 2014; 15:7124–7138.
28. Park JW, Kim JH, Kim SK, et al. A prospective evaluation of ^{18}F-FDG and ^{11}C-acetate PET/CT for detection of primary and metastatic hepatocellular carcinoma. J Nucl Med. 2008; 49:1912–1921. [PubMed: 18997056]
29. Trojan J, Schroeder O, Raedle J, et al. Fluorine-18 FDG positron emission tomography for imaging of hepatocellular carcinoma. Am J Gastroenterol. 1999; 94:3314–3319. [PubMed: 10566736]
30. Talbot JN, Fartoux L, Balogova S, et al. Detection of hepatocellular carcinoma with PET/CT: a prospective comparison of ^{18}F-fluorocholine and ^{18}F-FDG in patients with cirrhosis or chronic liver disease. J Nucl Med. 2010; 51:1699–1706. [PubMed: 20956466]
31. Delbeke D, Pinson CW. ^{11}C-acetate: a new tracer for the evaluation of hepatocellular carcinoma. J Nucl Med. 2003; 44:222–223. [PubMed: 12571213]
32. Ho CL, Yu SC, Yeung DW. ^{11}C-acetate PET imaging in hepatocellular carcinoma and other liver masses. J Nucl Med. 2003; 44:213–221. [PubMed: 12571212]
33. Ho CL, Chen S, Yeung DW, Cheng TK. Dual-tracer PET/CT imaging in evaluation of metastatic hepatocellular carcinoma. J Nucl Med. 2007; 48:902–909. [PubMed: 17504862]
34. Larsson P, Arvidsson D, Bjornstedt M, et al. Adding ^{11}C-acetate to ^{18}F-FDG at PET Examination Has an Incremental Value in the Diagnosis of Hepatocellular Carcinoma. Mol Imaging Radionucl Ther. 2012; 21:6–12. [PubMed: 23487415]

35. Cheung TT, Ho CL, Lo CM, et al. ^{11}C-acetate and ^{18}F-FDG PET/CT for clinical staging and selection of patients with hepatocellular carcinoma for liver transplantation on the basis of Milan criteria: surgeon's perspective. J Nucl Med. 2013; 54:192–200. [PubMed: 23321459]
36. Vavere AL, Kridel SJ, Wheeler FB, Lewis JS. 1-^{11}C-acetate as a PET radiopharmaceutical for imaging fatty acid synthase expression in prostate cancer. J Nucl Med. 2008; 49:327–334. [PubMed: 18199615]
37. Brown M, Marshall DR, Sobel BE, Bergmann SR. Delineation of myocardial oxygen utilization with carbon-11-labeled acetate. Circulation. 1987; 76:687–696. [PubMed: 3113765]
38. Buxton DB, Schwaiger M, Nguyen A, et al. Radiolabeled acetate as a tracer of myocardial tricarboxylic acid cycle flux. Circ Res. 1988; 63:628–634. [PubMed: 3136951]
39. Yoshimoto M, Waki A, Yonekura Y, et al. Characterization of acetate metabolism in tumor cells in relation to cell proliferation: acetate metabolism in tumor cells. Nucl Med Biol. 2001; 28:117–122. [PubMed: 11295421]
40. Schug Z, Peck B, Jones D, et al. Acetyl-coA synthetase 2 promotes acetate utilization and maintains cell growth under metabolic stress. Cancer Metab. 2014; 2(Suppl 1):O9.
41. Yoshii Y, Waki A, Furukawa T, et al. Tumor uptake of radiolabeled acetate reflects the expression of cytosolic acetyl-CoA synthetase: implications for the mechanism of acetate PET. Nucl Med Biol. 2009; 36:771–777. [PubMed: 19720289]
42. Yun M, Bang SH, Kim JW, et al. The importance of acetyl coenzyme A synthetase for ^{11}C-acetate uptake and cell survival in hepatocellular carcinoma. J Nucl Med. 2009; 50:1222–1228. [PubMed: 19617323]
43. Ho C, Wang C, Mattu S, et al. AKT (v-akt murine thymoma viral oncogene homolog 1) and N-Ras (neuroblastoma ras viral oncogene homolog) coactivation in the mouse liver promotes rapid carcinogenesis by way of mTOR (mammalian target of rapamycin complex 1), FOXM1 (forkhead box M1)/SKP2, and c-Myc pathways. Hepatol. 2012; 55:833–845.
44. Tward AD, Jones KD, Yant S, et al. Distinct pathways of genomic progression to benign and malignant tumors of the liver. Proc Natl Acad Sci USA. 2007; 104:14771–14776. [PubMed: 17785413]
45. Ponde DE, Dence CS, Oyama N, et al. ^{18}F-fluoroacetate: a potential acetate analog for prostate tumor imaging--in vivo evaluation of 18F-fluoroacetate versus ^{11}C-acetate. J Nucl Med. 2007; 48:420–428. [PubMed: 17332620]
46. Chen X, Calvisi DF. Hydrodynamic transfection for generation of novel mouse models for liver cancer research. Am J Pathol. 2014; 184:912–923. [PubMed: 24480331]
47. Li L, Wang C, Calvisi DF, et al. SCD1 Expression is dispensable for hepatocarcinogenesis induced by AKT and Ras oncogenes in mice. PLoS One. 2013; 8:e75104. [PubMed: 24069385]
48. Bederman IR, Foy S, Chandramouli V, et al. Triglyceride synthesis in epididymal adipose tissue: contribution of glucose and non-glucose carbon sources. J Biol Chem. 2009; 284:6101–6108. [PubMed: 19114707]
49. Hsieh CW, Millward CA, DeSantis D, et al. Reduced milk triglycerides in mice lacking phosphoenolpyruvate carboxykinase in mammary gland adipocytes and white adipose tissue contribute to the development of insulin resistance in pups. J Nutr. 2009; 139:2257–2265. [PubMed: 19812223]
50. Brunengraber DZ, McCabe BJ, Kasumov T, et al. Influence of diet on the modeling of adipose tissue triglycerides during growth. Am J Physiol Endocrinol Metab. 2003; 285:E917–925. [PubMed: 12799315]
51. Patlak CS, Blasberg RG. Graphical evaluation of blood-to-brain transfer constants from multiple-time uptake data. Generalizations. J Cereb Blood Flow Metab. 1985; 5:584–590. [PubMed: 4055928]
52. Czernin J, Weber WA, Herschman HR. Molecular imaging in the development of cancer therapeutics. Annu Rev Med. 2006; 57:99–118. [PubMed: 16409139]
53. Lee SA, Ladu S, Evert M, et al. Synergistic role of Sprouty2 inactivation and c-Met up-regulation in mouse and human hepatocarcinogenesis. Hepatol. 2010; 52:506–517.
54. Giordano S, Columbano A. Met as a therapeutic target in HCC: facts and hopes. J Hepatol. 2014; 60:442–452. [PubMed: 24045150]

55. Czernin J, Benz MR, Allen-Auerbach MS. PET Imaging of Prostate Cancer Using ^{11}C-Acetate. PET Clinics. 2009; 4:163–172. [PubMed: 21984877]

56. Salem N, Kuang Y, Corn D, et al. [(Methyl)1-(11)C]-acetate metabolism in hepatocellular carcinoma. Mol imaging Biol. 2011; 13:140–151. [PubMed: 20401538]

57. Cheung TT, Chan SC, Ho CL, et al. Can positron emission tomography with the dual tracers [^{11}C]acetate and [^{18}F]fludeoxyglucose predict microvascular invasion in hepatocellular carcinoma? Liver Transplant. 2011; 17:1218–1225.

58. Hwang KH, Choi DJ, Lee SY, et al. Evaluation of patients with hepatocellular carcinomas using [(11)C]acetate and [(18)F]FDG PET/CT: A preliminary study. Appl Radiat Isotop. 2009; 67:1195–1198.

59. Hu S, Balakrishnan A, Bok RA, et al. 13C-pyruvate imaging reveals alterations in glycolysis that precede c-Myc-induced tumor formation and regression. Cell Metab. 2011; 14:131–142. [PubMed: 21723511]

60. Huynh H, Soo KC, Chow PK, Tran E. Targeted inhibition of the extracellular signal-regulated kinase kinase pathway with AZD6244 (ARRY-142886) in the treatment of hepatocellular carcinoma. Mol Cancer Ther. 2007; 6:138–146. [PubMed: 17237274]

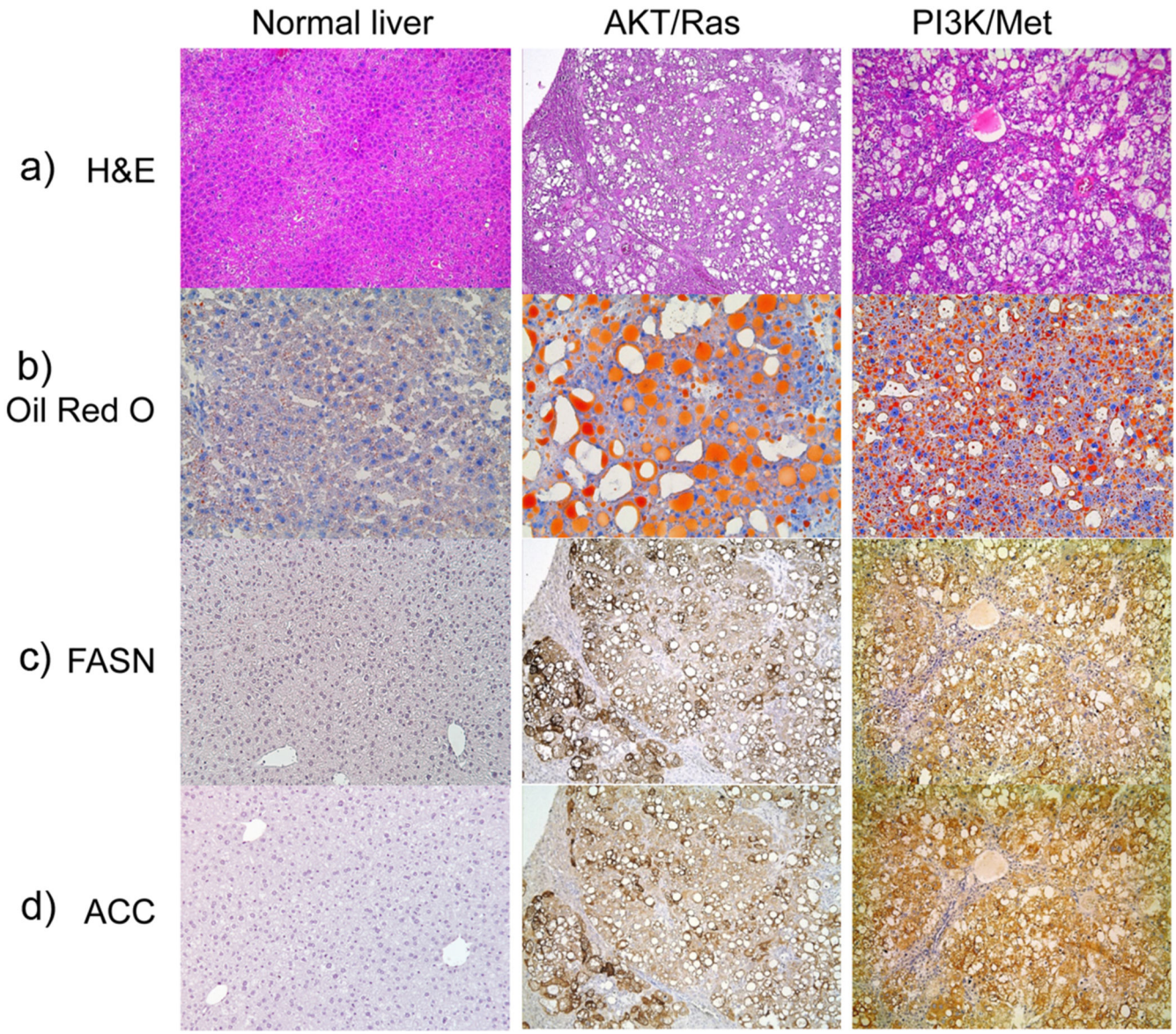

Figure 1.

Increased lipid droplet accumulation and *de novo* fatty acid biosynthesis protein levels in AKT/Ras and PI3K/Met mouse liver tumor samples. **a)** H&E staining; **b)** Oil Red O staining; **c)** Immunostaining of FASN; **d)** Immunostaining of ACC. Original magnification: 200× in Oil Red O staining; 100× in all the other pictures.

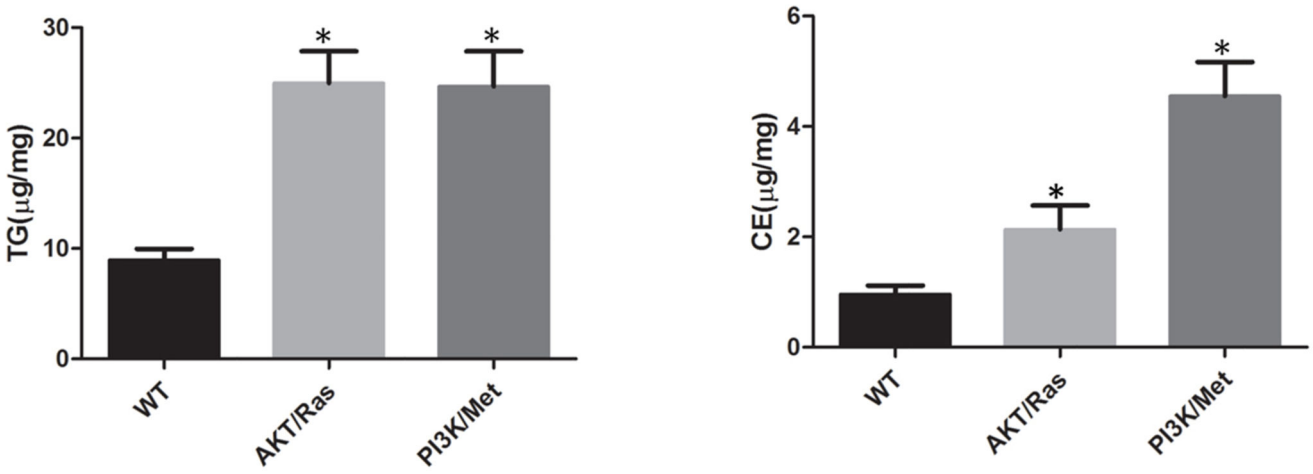

Figure 2.

Total amount of **a)** triglycerides and **b)** cholesterol esters in wild type livers (n = 6), AKT/Ras (n = 4) and PI3K/Met (n = 4) liver tumors. Data are presented as median ± SEM. *, $p < 0.05$ versus wildtype normal liver control.

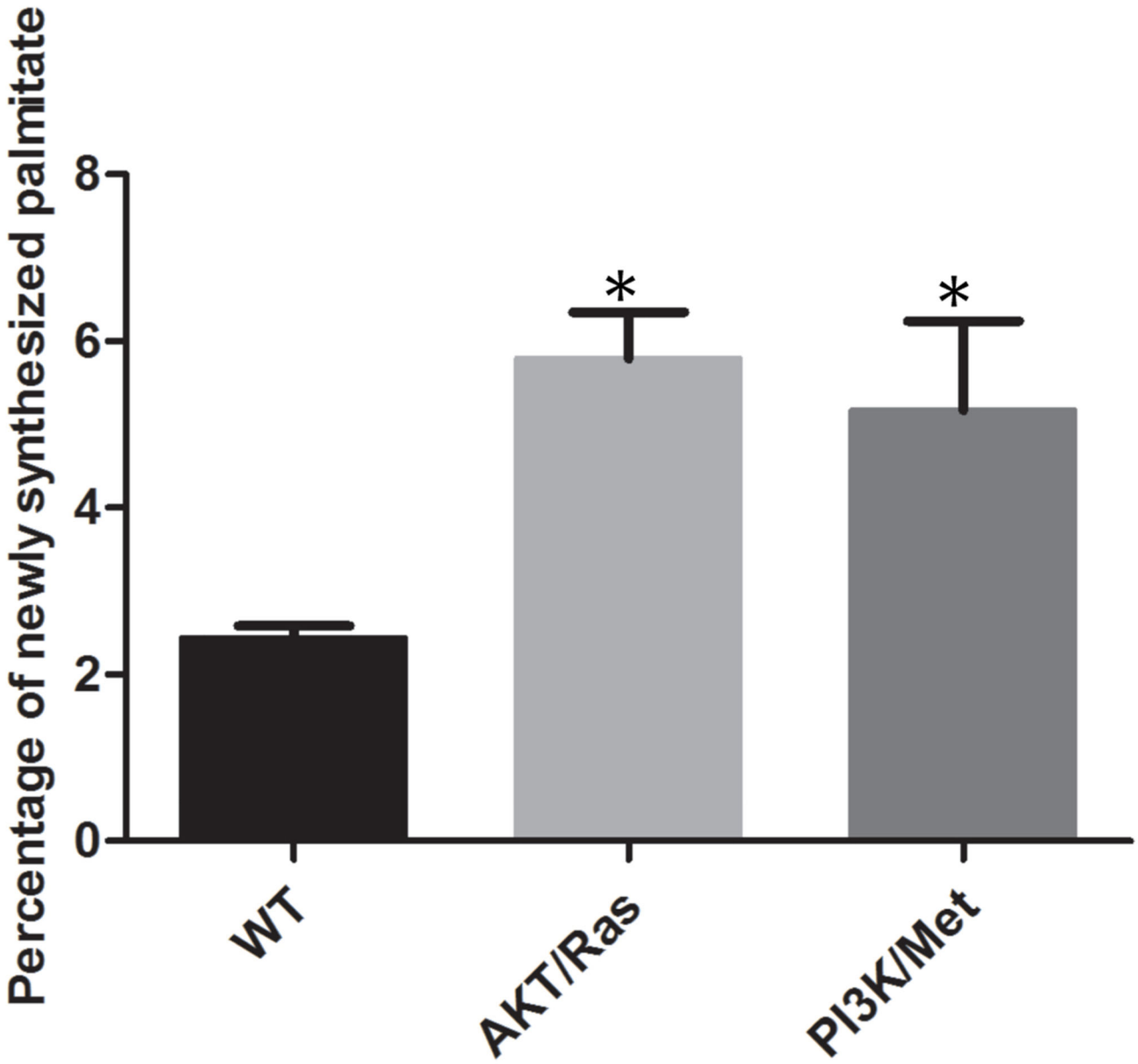

Figure 3.

De novo lipogenesis rate in wild type livers (n = 6), AKT/Ras (n = 4) and PI3K/Met (n = 5) mouse liver tumor samples measured by ^{2}H incorporation in palmitate.

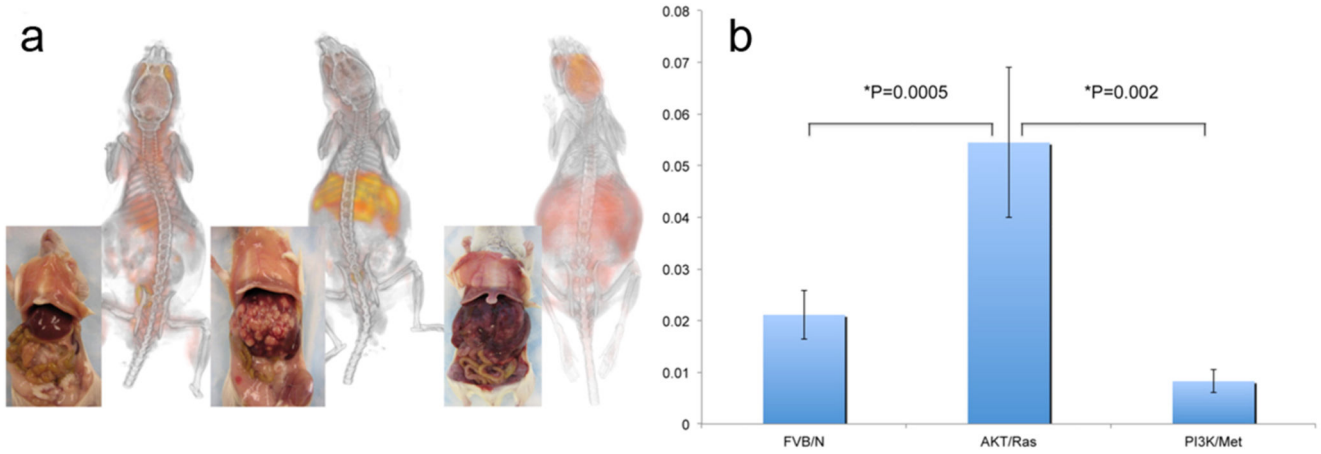

Figure 4.

a) 3D volume rendering of [^{11}C]acetate K_i distributions of representative FVB/N (left), AKT/Ras (middle), and PI3K/Met (right) mice. Insets show the presence of tumors or normal livers. **b)** Influx rate constants (K_i's) values measured from *in vivo* dynamic [^{11}C]acetate PET/CT imaging in normal liver (FVB/N), Akt/Ras and PI3K/Met liver tumors. P values indicate that the comparison between these three pairs was statistically significant.